Journal of Geosciences and Geomatics, 2019, Vol. 7, No. 1, 42-53
Available online at http://pubs.sciepub.com/jgg/7/1/5
Published by Science and Education Publishing
DOI:10.12691/jgg-7-1-5

Using EGM2008 Gravity Data for Mapping and Detecting Structural Subsurface Anomalies in the Mayo-Kani Division (Cameroon)

Jean Jacques Nguimbous-Kouoh[1,*], Simon Ngos III[1], Eliezer Manguelle-Dicoum[2]

[1]Department of Mines, Petroleum, Gas and Water Resources Exploration, Faculty of Mines and Petroleum Industries, University of Maroua, P.O. Box 08 Kaele, Cameroon
[2]Department of Physics, Faculty of Science, University of Yaoundé I, PO Box 6052 Yaoundé, Cameroon
*Corresponding author: nguimbouskouoh@yahoo.fr

Received January 01, 2019; Revised February 03, 2019; Accepted February 10, 2019

Abstract To resolve the problem of gravity mapping in the Mayo-Kani Division, we extracted a sample of data from the high-resolution Bouguer anomaly database EGM2008. The objective of this process was to map and detect subsurface anomalies in the region. Regional-residual separation was applied to the data using a third-order polynomial fit. This separation enables to obtain regional and residual maps. Other filtering actions, such as horizontal and vertical derivatives, have been applied to the data to enhance sources of anomalies in the study area. The residual map of the study area was superimposed on the geological map to delineate and interpret the correlation with the shallow geological structures. The main sources of residual gravity anomalies have been recognized. The interpretation of the derived maps revealed the N-S, E-W, NE-SW and NW-SE structural patterns. These trends have been associated with the major structural directions observed in the Far North Cameroon region. The Euler Deconvolution allowed the detection of sources of anomalies and to determine their depths. The fracture map obtained from this method has improved knowledge on the search for buried ores and the geological structures associated with oil and gas deposits. Overall, the generated gravity maps provided a better understanding of the Mayo-Kani geological setting.

Keywords: *EGM2008, polynomial fitting, Euler Deconvolution, gravity mapping, Mayo-Kani*

Cite This Article: Jean Jacques Nguimbous-Kouoh, Simon Ngos III, and Eliezer Manguelle-Dicoum, "Using EGM2008 Gravity Data for Mapping and Detecting Structural Subsurface Anomalies in the Mayo-Kani Region (Cameroon)." *Journal of Geosciences and Geomatics*, vol. 7, no. 1 (2019): 42-53. doi: 10.12691/jgg-7-1-5.

1. Introduction

Satellite mapping has for some time been making great progress and success in the search for buried ores and structures associated with oil or gas deposits [1,2,3]. It is achieved by linking the points, by interpolation or reasoned extrapolation of the unknown. It is from satellite mapping that maps are made using approaches evolving scientific concepts, supported by more and more efficient analytical means. Because of this, the states can have information to stimulate exploration activities, then exploitation of their mineral raw materials and thus contribute to the development of their economies [1,2,3]. Given the importance of satellite mapping for certain states, we have decided in this study to approach the gravity mapping of the Mayo-Kani Division. Indeed, in this region the terrestrial and aerial data do not exist. Various authors, however, suggest that gravity data derived from the gravity model EGM2008 can be used effectively to compensate for the absence and rarity of terrestrial and aerial gravity data [4-11]. Generally, the exercise consists of simply extracting the data from this model over a range of interest. In this paper we use data from the high resolution geo-potential model EGM2008 for mapping anomalies of the Mayo-Kani Division and delineating geological structures that have a high mineralogical or petroleum potential. The high resolution geo-potential model EGM2008 used is derived from the EGM96 model that is published every decade. The gravity data from this model have an important aspect [4-11]: they are less expensive and allow a quick and general coverage in less time of large areas of exploration. The interpretation of these data is generally a very vital tool in the mineral and/or petroleum exploration industry by identifying anomalies and lineaments. The maps from the EGM2008 model are dependent on the ability of the devices installed within the satellites to detect slight variations in the density of the rocks in the subsurface. The resolution of these devices and their orientation may allow better detection of anomalies and fractured structures of the soil and subsoil.

The article consists of five parts: the geological context of the study area, the source of the EGM2008 data, the filtering methods, the interpretation of the obtained maps and discussion.

2. Geologic Setting

The Mayo-Kani Division, is one of the six Divisions of Far-North Region of Cameroon. The geological history of this study area and the Far-North Region of Cameroon (Figure 1) is closely related to that of the Lake Chad Basin [12,13,14]. In this region, sedimentary deposits are dependent on a succession of regression and transgression regimes caused by the alternation of arid and wet periods [12,14-18]. The major structural directions encountered here are [14,16,18-23]: N12°E, N28°E: Cameroon volcanic line, N58°E: Somali direction, N73°E: Adamawa line, N117°E, N135°E to 142°E: Eritrean direction. These directions control the folding and faulting of crystallophyllian basement rocks, the location of volcanic and subvolcanic devices, and the ultimate post-tectonic intrusive massifs and much later the hydrographic network. The basement rocks are Precambrian in age and have been reactivated during the Pan-African orogeny (~600 Ma) and this signature makes it possible to integrate the local geological evolution and structural framework of the Far-North of Cameroon in a global context [14,16,18-23].

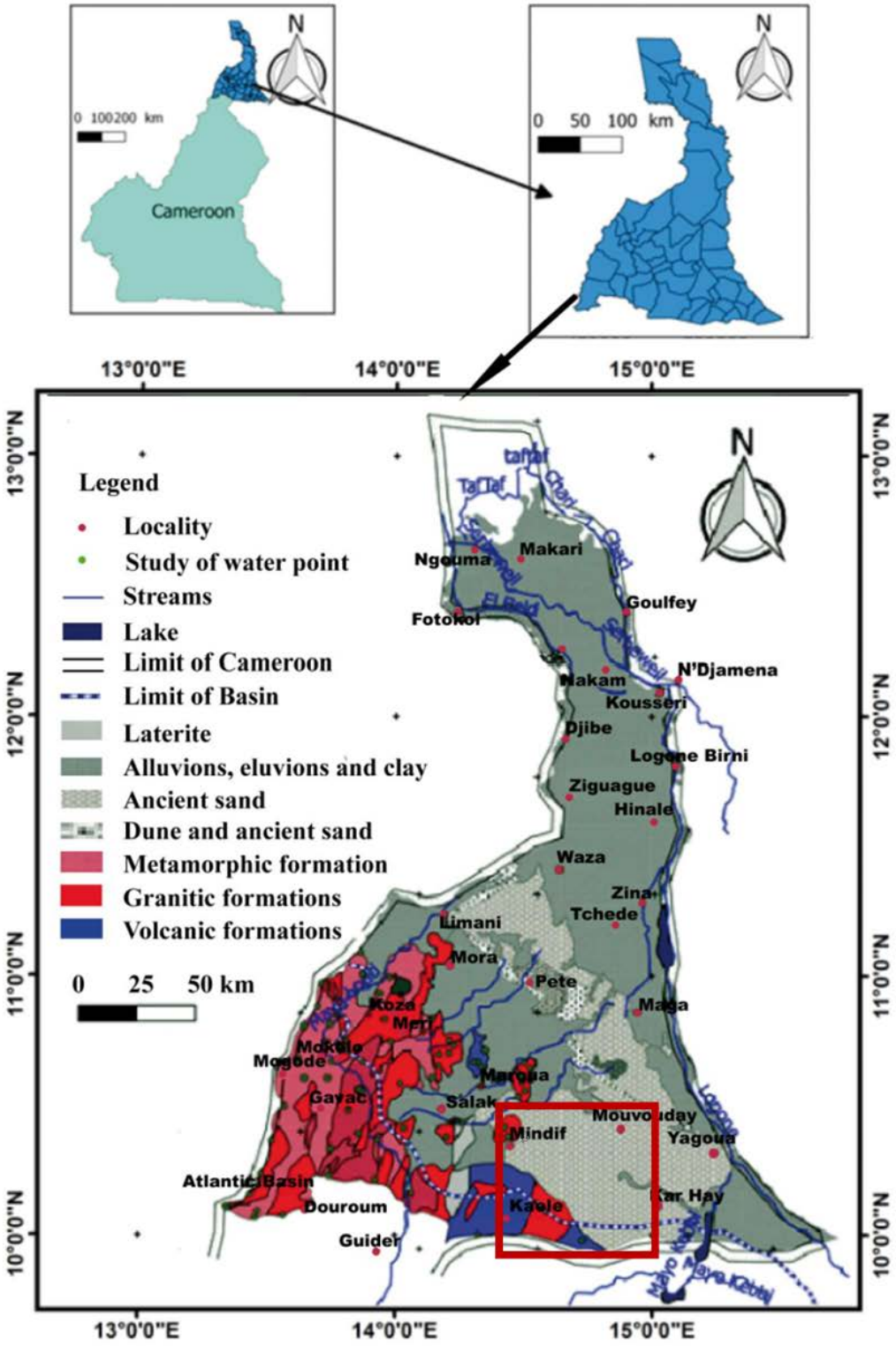

Figure 1. Geological map of the Far-north of Cameroon, the red frame contains the Mayo-Kani zone [12,13,14]

Far-North Region of Cameroon (Figure 1) is represented by Precambrian crystallophyllian basement rocks, sedimentary formations and volcanic formations [12,13,14]. In this region, the Precambrian crystalline basement outcrops continuously in the mountainous western areas, the Southeast peneplain sporadically, and inselberg in the central zone [12,13,14]. This basement consists of three main units [12,14,16,18-23]: an epi-metamorphic complex covering most of the northern part and forming a band to north of Maroua; a migmatitic meso-metamorphic ensemble covering about 50% of the basement surface and forming with the granites all of the Mandara Mountains; a non-migmatitic meso-metamorphic ensemble covering about 10% of the surface of the basement flush in the Kaele peneplain and Moutourwa. The sedimentary formations extend from the foot of the Mandara Mountains to the eastern Diamare Plain; all this together constitutes the sedimentary cover; its thickness varies from a few meters at the foothills to several tens of meters at Lake Chad [12,13,14]. These are mainly lacustrine clays and ancient sands overlain by alluvia from the Logone river and the Mandara Mountains.

In more detail, sedimentary rocks such as alluvium, clay, limestone and sandstone make up most of the surficial rocks of the Far-North Region [12,14,16,18-26]. These deposits follow the rivers of the region, such as Logone and Mayo Tsanaga, which flow into Lake Chad in the north. In the south of the region, a strip of granite separates the sedimentary zone from an area of metamorphic rock located to the southwest. The latter region includes outcrops of micaceous gneiss and shale (Figure 1). The Rhumsiki Valley, a mountainous field littered with extinct volcano cones and necks, is a small area of volcanic rock, such as trachyte and rhyolite. The soils in this region are a bit more complex. They are dominantly young soils rich in raw minerals. This is the case for much of the land south of Lake Chad and the Mandara Mountains on the western border with Nigeria [18-26]. Here, the soil consists mainly of black clay (alluvial soil). The seasonal floods of the Logone River give rise to a north-south band of hydromorphic soils on the Chadian border. The rest of the territory, comprising the Diamare plain and the river El Beïd valley, consists of ferruginous soils. Seasonal wet/dry variations in the region create relatively shallow, ferrous or lateritic soils [18-26].

In terms of relief, most of the Far-North Region of Cameroon is at a relatively low altitude. This low part forms portion of the Lake Chad plain and its gentle slopes vary from 500 m in the southwest to 200 m at the edge of the Logone river. The average elevation of this basin is 280 m (Figure 1). The Diamare plain occupies the lower third of the Lake Chad plain and is characterized by a number of isolated inselbergs. The Mandara Mountains on the southwestern border with Nigeria form the highest point, between 500 m to 1000 m above sea level, with an average of about 900 m [18-26]. The Tourou Mountain is the highest point culminating at 1442 m. These mountains are probably the result of the same tectonic activity that led to the Benue trough in Nigeria. The area was once volcanically active, as evidenced by a number of trachyte and rhyolite extrusions of extinct volcanoes. The most spectacular of them is in the valley near the tourist village of Rhumsiki. The part of the chain located in the far-north is on a medium plateau located between 800 m and 900 m. Isolated mountains continue in the Diamare plain, at Mindif, Boboyo, Kaele and Lara. The northern expanse of these mountains is dissected by several rivers [18-26].

The study area (Figure 2) is located in the far-north of Cameroon. It is bounded by latitudes (9.50°N-10.40°N) and longitudes (14.00°E-15.50°E). This area is covered with sedimentary formations and magmatic formations represented by a set of isolated and chaotic rock masses. The geological formations generally listed are [27]: granites, sandy clays, micaschists, clay sands, laterite, basalts and rhyolites.

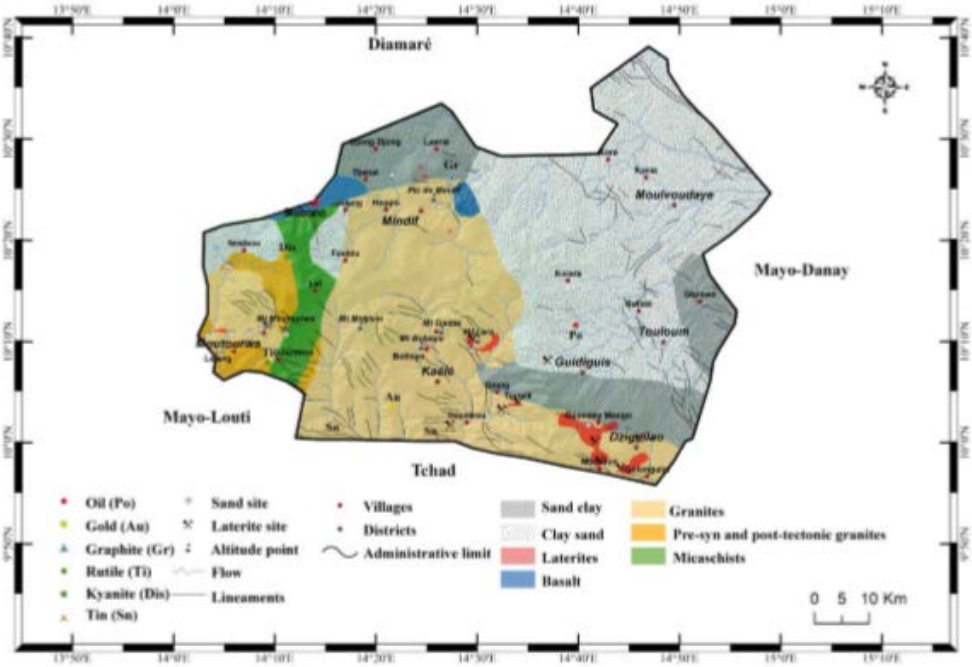

Figure 2. Geological map of Mayo-Kani: [27], it allows making a mining inventory of the study area. It includes a legend that lists and describes the geological formations that one meets there

The geological maps that we have just described (Figure 1 and Figure 2) enable to make a mining inventory of the region. They include a legend that lists and describes the formations found there. These formations are a projection on the topographic surface, of the rock layers organization in depth. The realization of these maps was based on the "entities" recognition that make up the subsurface and on the geological formation's geographical distribution and their mutual relations.

3. Data Origin

The Bouguer gravity data used in this study were extracted from the Earth Geospatial Model (EGM 2008) from which the World Gravity Map (WGM) was produced. The authors of these data are NGA, AGI and IGFS. The information contained in these data includes longitudes, latitudes, altitudes, the free-air gravity values observed and corrected Bouguer gravity values. This gravity dataset comprehensively covers the entire world and has undergone the best possible corrections to date [4-11,28,29,30,31,32]. Bouguer corrections were made with a density of 2.670 kg/m^3. We use this data because it can cover a larger area than land and air data. They can correct systematic errors in land surveys. The equipment, techniques, software and treatment procedures are already established and in development. The EGM2008 model has several advantages [4-11,28,29,30,31,32]: (1) It uses an ellipsoidal harmonic coefficient of 2160 (11km); (2) It has the highest spatial resolution available and a uniform gravity data capability; (3) It has been well developed and is free to use. It can solve problems related to a spatial resolution of five minutes arc or nine kilometers for most regions, a resolution about six times higher than previous models. (4) It provides good information on previously inaccessible or poor-data areas and extends across natural and man-made boundaries. (5) It integrates data from different sources, including satellite altimetry on the oceans and Earth's gravity.

The absolute gravity values of the EGM2008 model were calculated using the Geosoft Oasis-Montaj software [33]. The World Geodetic System 1984was used to calculate the gravity value on the Earth's ellipsoid [4-11,33]:

$$g_0 = 9.7803267714\left(\frac{1+0.001931855138639\sin^2\lambda}{\sqrt{1-0.00669437999013\sin^2\lambda}}\right)$$

where λ is the latitude of the gravity station.

The different authoring agencies of this data applied the latitude, altitude, topography, bouguer, free-air and Eotvos corrections [4-11,33]. The map (Figure 3) represents the regular digitized grid of study area data extracted from the EGM2008 model.

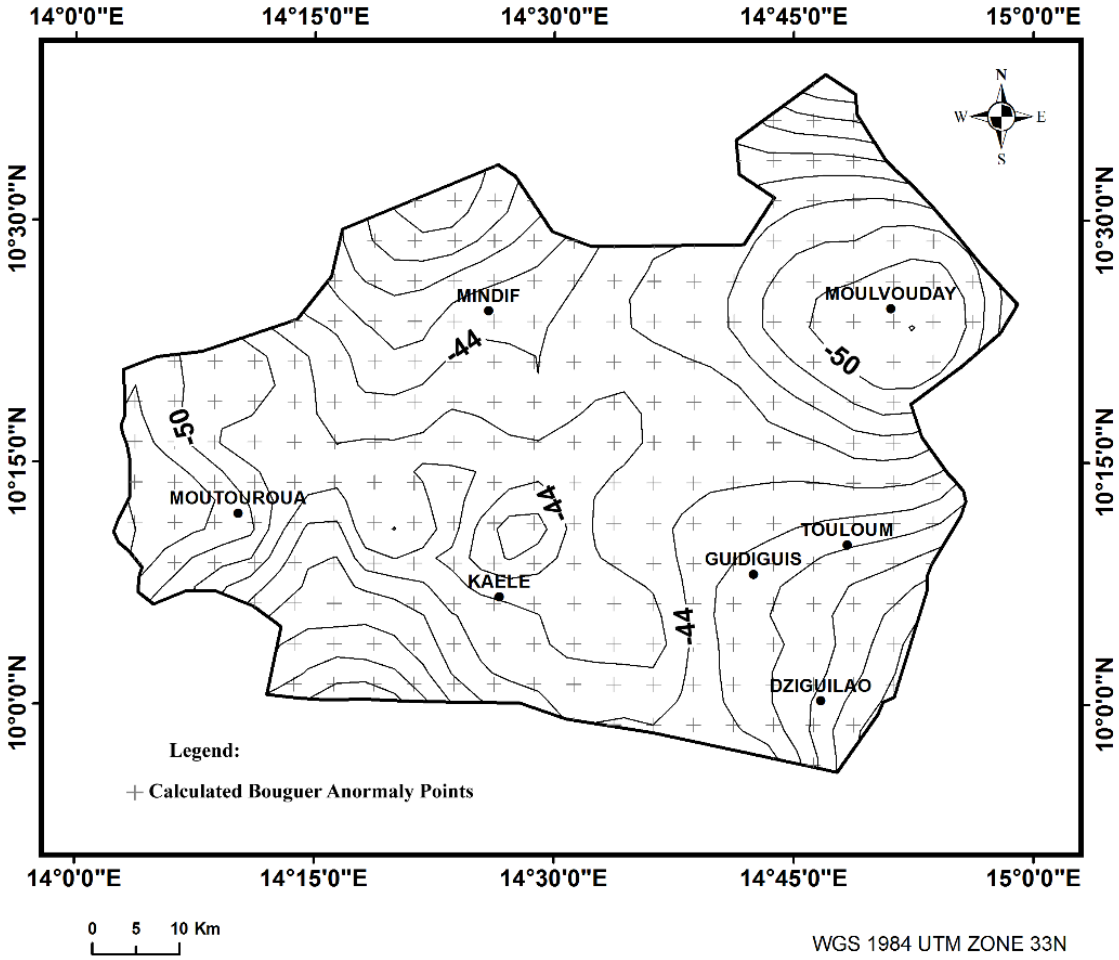

Figure 3. Bouguer data post map,the data were integrated into the Surfer software and tied to the World Reference Geodetic System (WGS84) using Manoca 1962 UTM zone 33N projection

4. Methods

To facilitate geophysical interpretation, several filtering techniques have been applied to gravity data. These filters have been applied using the Oasis Montaj software and are considered most useful for delineating gravity anomalies, defining body edges, and amplifying trends in terrestrial discontinuities [4-11,33]. Regional-residual separation by analytical polynomial fit was applied to the EGM2008-Bouguer data. Gradient filters were applied to detect sources of anomalies and enhance structural directions. Euler's deconvolution was applied to localize sources of local anomalies, deduce their depths, and obtain the fracture map of the study area.

4.1. Polynomial Fitting Method

The polynomial fit was used to produce the third-order regional and residual maps using the Oasis Montaj software [33]. This method is based on polynomial decomposition series. It uses the least squares method to compute the mathematical surface giving the best fit to the data for a specified degree of detail [33,34,35,36]. This surface is considered the regional gravity anomaly. The residual is obtained by subtracting the regional field from the Bouguer gravity field. In practice, the regional surface is considered as two-dimensional polynomial. The order of this polynomial depends on the complexity of the geology of the study area [33,34,35,36]. The third order polynomial surfaces of the regional anomaly obtained in this work are presented along with the corresponding residual anomaly.

4.2. Horizontal and Vertical Derivatives Methods

The horizontal and vertical derivatives have been used to enhance and highlight the edge of the anomalies, and to move the maximum number of anomalies above the sources. They have also been used to define trends and boundaries of structures and to separate anomalies at varying frequencies [37-41]. Horizontal and vertical derivatives are often used for qualitative interpretations as they prove to be a very effective means of highlighting short wavelength anomalies [37-41]. The horizontal derivatives bring out lineaments perpendicular to the direction of the derivation. Whereas, vertical derivatives focus on superficial sources [37-41]. The basic equations of these derivatives obey the Fourier transforms in order n $\left(F\left[\frac{d^nG}{dx^n}\right]\right)$ in the frequency domain. The Fourier transform of the derivatives is calculated by multiplying the Fourier transform of the field F[G] by the wave numbers (kx, ky and k). The equations for these derivatives are formulated as follows [37-41]:

$$F\left[\frac{dG}{dx}\right]=ik_xF[G];F\left[\frac{dG}{dy}\right]=ik_yF[G]$$

$$and\ F\left[\frac{dG}{dz}\right]=|k|F[G]$$

Where n = 1 is the degree of derivation and i is the imaginary number ($i^2=-1$).

4.3. Euler Deconvolution Method

The application of Euler deconvolution to gravity geospatial data often leads to very interesting results for mapping. It uses the gravity field to locate the sources of anomaly and thus allow to quickly obtain an estimate of the source's depth [42-51]. Initially developed for the interpretation of aeromagnetic and aerogravity data, Euler's Deconvolution uses the three components of the gravity field gradient (two horizontal and one vertical) to locate sources of anomaly [42-51]. This method enables to quickly obtain an estimate of the source's depth. The data of the gravity field to be interpreted, G, are interpolated on a regular grid and the gradients are calculated from this grid (Figure 3). The estimation of the observed regional field, G_0, and of the structural index, N, which characterizes the type of source, are fundamental for a good application of the method.

4.3.1. Formulation of the Euler Deconvolution

Euler's deconvolution is based on the mathematical formulation represented by the following homogeneity equation (42,43,46]:

$$G(x,y,z)=\frac{k}{\sqrt{\left[(x-x_o)^2-(y-y_0)^2-(z-z_0)^2\right]^N}}$$

With: G the intensity of the field of anomalies at the point (x, y, z); (x_0,y_0,z_0) the geologic location coordinates of the anomaly source; k a parameter independent of (x, y, z) and N the structural index. In the case of gravity data, N can take the values 0, 1, 2 (N = 0 for contacts and faults, N = 1 for dykes, N = 2 for horizontal or vertical cylinders). Using the one order upwind discretization scheme, the Euler homogeneity equation of the previous gravity field becomes:

$$G_{ijk}=\frac{\begin{bmatrix}\Delta y\Delta z(x-x_0)G_{i+1,j,k}+\Delta x\Delta z(y-y_0)G_{i,j+1,k}\\+\Delta x\Delta y(z-z_0)G_{i,j,k+1}-\Delta x\Delta y\Delta zNG_0\end{bmatrix}}{\begin{bmatrix}\Delta y\Delta z(x-x_0)+\Delta y\Delta z(x-x_0)\\+\Delta y\Delta z(x-x_0)-\Delta x\Delta y\Delta zN\end{bmatrix}}$$

With Δx, Δy and Δz the different increments along the x, y and z directions.

The matrix scheme of the Euler homogeneity equation used is of the form:

$$\begin{bmatrix}\frac{\partial G}{\partial x_1} & \frac{\partial G}{\partial y_1} & \frac{\partial G}{\partial z_1} & N\\ \vdots & \vdots & \vdots\ \vdots & \\ \vdots & \vdots & \vdots\ \vdots & \\ \frac{\partial G}{\partial x_n} & \frac{\partial G}{\partial y_n} & \frac{\partial G}{\partial z_n} & N\end{bmatrix}\begin{bmatrix}\\ x_0\\ y_0\\ z_0\\ G_0\end{bmatrix}$$

$$=\begin{bmatrix}x_1\frac{\partial G}{\partial x_1} & y_1\frac{\partial G}{\partial y_1} & z_1\frac{\partial G}{\partial z_1} & NG_1\\ \vdots & \vdots & \vdots\ \vdots & \\ \vdots & \vdots & \vdots\ \vdots & \\ x_n\frac{\partial G}{\partial x_n} & y_n\frac{\partial G}{\partial y_n} & z_n\frac{\partial G}{\partial z_n} & NG_n\end{bmatrix}.$$

To solve this system of equations, it takes at least four measurement points. For this we consider a square window (w x w = n) on the gradient grids of the field. This window gives a system of n linear equations [42,43,46]. By representing the matrix system in the form: $AM = D$, the matrix of solutions M is obtained in the form: $M = A^{-1}D$ in the least-squares sense, with A^{-1} the inverse matrix of A.

5. Results and Interpretation

We distinguish two types of interpretations of gravity data; qualitative interpretation and quantitative interpretation. Here we present a qualitative interpretation of gravity anomaly maps.

5.1. Qualitative Interpretation of Fitting Gravity Maps

In this part, we interpret the Bouguer Gravity anomaly maps, regional and residual. This interpretation aims to establish correlations between gravity maps and the geology of the area. The tectonics of the study area can be examined by analyzing the structural trends of the different color scales.

5.1.1. Interpretation of the Bouguer Anomaly Map

The EGM2008 mesh gravity data map (Figure 3) produced the Bouguer anomaly map (Figure 4). The analysis carried out on this map according to the color's amplitude allow to recognize the shape, the size and the limits of the various abnormal forms. The color distribution represents a combination of shallow anomalies and deep-seated anomalies. Its description provides an aid to the delineation of heterogeneities created by geological formations due to density variations within the Earth's crust [47-51]. This color distribution shows two types of anomalies: red high-density anomalies that are associated with a high-density level and low-density green, blue, and yellow anomalies that are associated with a low-density level. The color scale reveals that the Bouguer field amplitude is 42 mGal varying between -65.6 and -24.1 mGal. Overall the different structures are oriented N-S, E-W, NW-SE and NE-SW. These directions control the folding of crystallophyllian rocks, faults, the hydrographic network, the location of volcanic and subvolcanic devices, and the ultimate post-tectonic intrusive massifs in the region.

5.1.2. Interpretation of the Regional Anomaly Map

The regional anomaly map (Figure 5) is considered to be close to the effect of very deep or regional structures at the local scale. The regional anomalies observed are characterized by large negative anomalies varying between -36.9 mGal and -47.8 mGal. It globally has a E-W gradient direction. This gradient corresponds to a thinning of the crust towards the north of the study area.

5.1.3. Interpretation of the Residual Anomaly Map

The EGM2008 residual anomaly map (Figure 6) shows anomaly values ranging from -22.6 mGal to 18.1 mGal, mainly grouped into positive (P) and negative (N) anomalies. It has four poles of colored anomalies: the positive anomalies of West Kaele, Mindif, North Moulvouday and Guidiguis, Touloum and Dziguilao. These positive red anomalies can be associated with magmatic inselbergs. The correlation of the residual map with the geological map shows that the negative anomalies of green, yellow and blue color correspond to an alternation of sedimentary formations such as clayey sand and sandy clays. Overall, the surface geological structures are oriented N-S, E-W, NW-SE and NE-SW which is an indication of the structural trending directions of subsurface and mineralogical traps or deposition of hydrocarbons in the region.

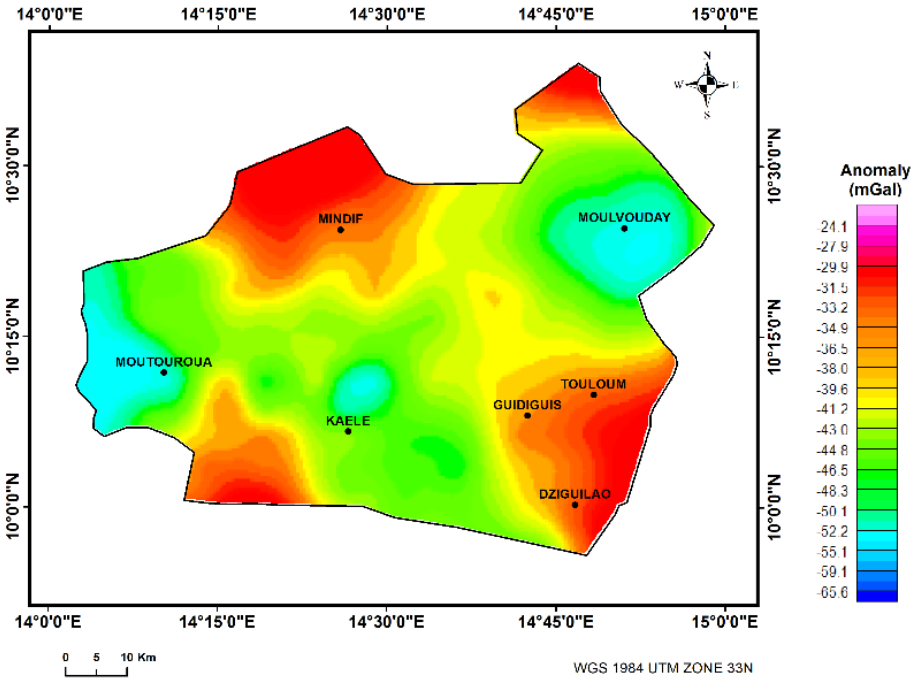

Figure 4. Bouguer anomaly map of the study area with high-densities marked in red and low-densities in yellow, green and blue

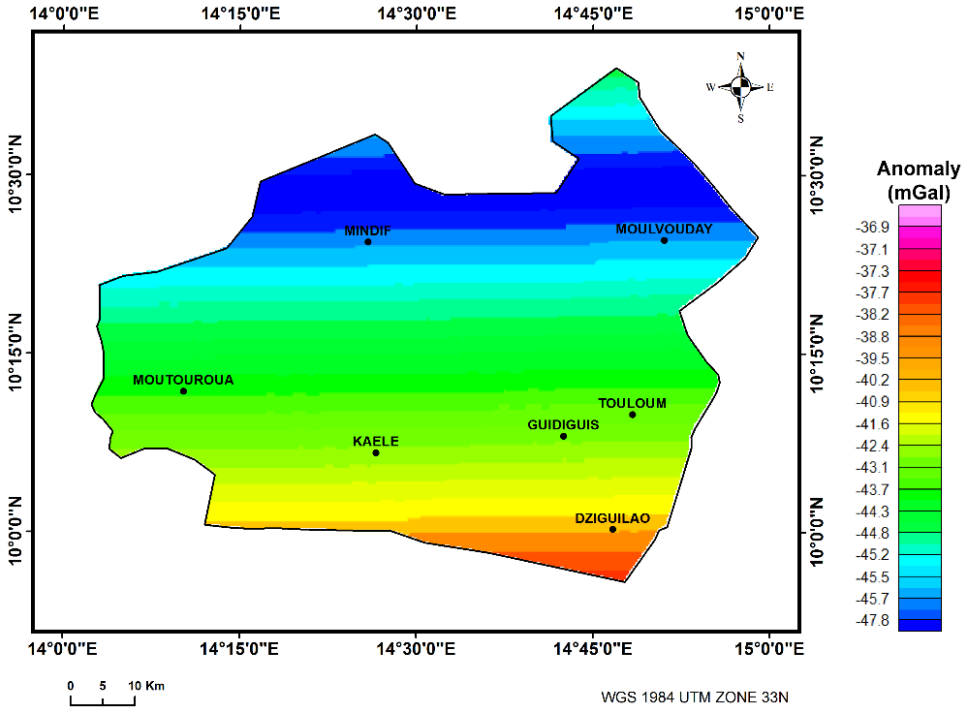

Figure 5. Map of regional anomalies of the study area marked by a strong horizontal gradient

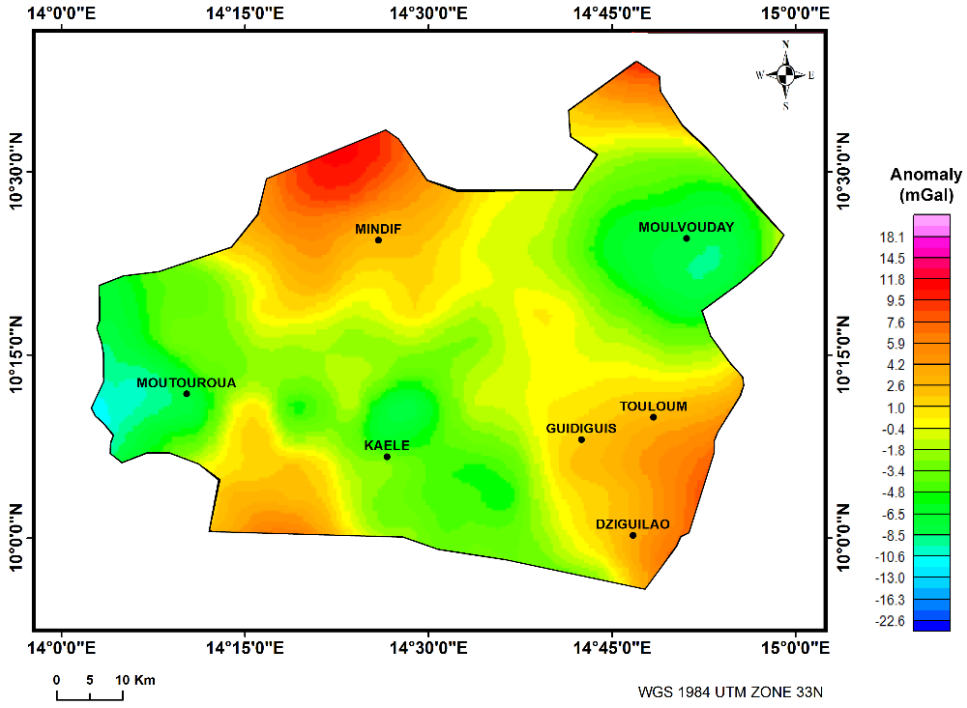

Figure 6. Map of residual gravity anomalies produced by subtracting a third-order polynomial surface from the Bouguer anomaly

5.2. Qualitative Structural Interpretation of Derivative Maps

To map the gravity lineaments of the study area, horizontal and vertical gradients were applied to the data. In this part we present the results in the form of anomaly maps.

5.2.1. Interpretation of the Horizontal Derivative Map According to X

Figure 7 is the map of the horizontal gradient along X. This map presents maxima and minima of gradient: The maxima gradients are marked in red color and can be associated with the trend direction of the basement formations; the green, yellow and blue minima gradients can be associated with discontinuities in sedimentary formations. The most important trends observed on the map are N-S and NE-SW directions. These trends coincide with the orientation of faults and geological contacts between basement formations and sedimentary formations. To obtain this map, the following characteristics were selected: the structural index N = 0, the window calculation WS = 10km x 10km and the tolerance T = 15%.

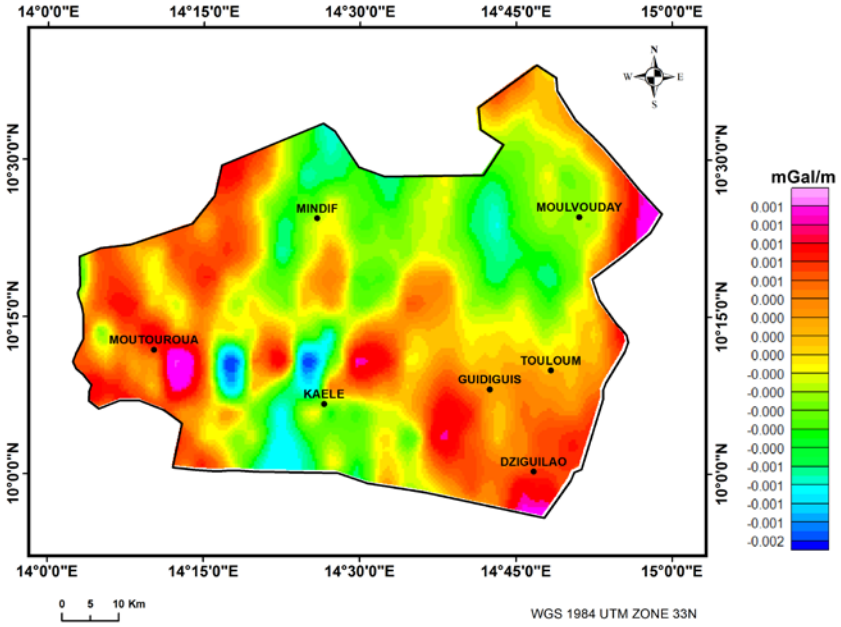

Figure 7. Horizontal gradient (X) gravity anomalies map with maxima gradients marked in red color and minima in green, yellow and blue color

5.2.2. Interpretation of the Horizontal Derivative Map According to Y

The map (Figure 8) represents the horizontal derivative along Y. This map also has maxima and minima gradient: the maxima gradients are marked in red and can be associated with the direction of the basement formations while the green, yellow and blue minima gradient can be associated with discontinuities in sedimentary formations. The most important trends observed are NW-SE and NE-SW directions. These trends coincide with the orientation of faults and geological contacts between the basement formations and the sedimentary formations of the study area, perpendicular to the derivation direction. To obtain this map, the following characteristics were selected: the structural index N = 0, the calculation window WS = 10km x 10km and the tolerance T = 15%.

5.2.3. Interpretation of the Vertical Derivative Map

The vertical derivative technique has almost the same objective as residual polynomial filtering in gravity data. It emphasizes the expression of local characteristics and suppresses the effects of regional anomalies [47-51]. The vertical derivative map (Figure 9) shows a colored distribution of the gravity anomaly across the Mayo-Kani Division. It highlights the abnormal effects close to the surface at the expense of the effects of deep origin. His analysis shows that it enhances the edges of anomalies and improves the superficial features. Small anomalies are more apparent in areas of strong regional disturbance. This map shows areas of high mineralization, particularly in Moutourwa and north of Kaele; at Moulvouday the anomaly in blue can be associated with the portion of a sedimentary basin.

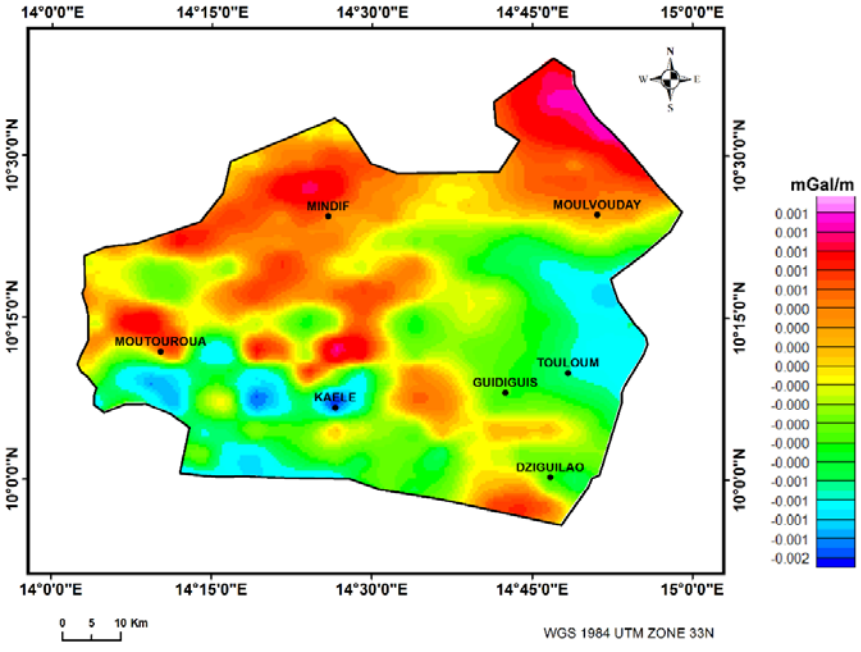

Figure 8. Horizontal gradient (Y) gravity anomalies map with the maxima gradients marked in red color and minima in green, yellow and blue.

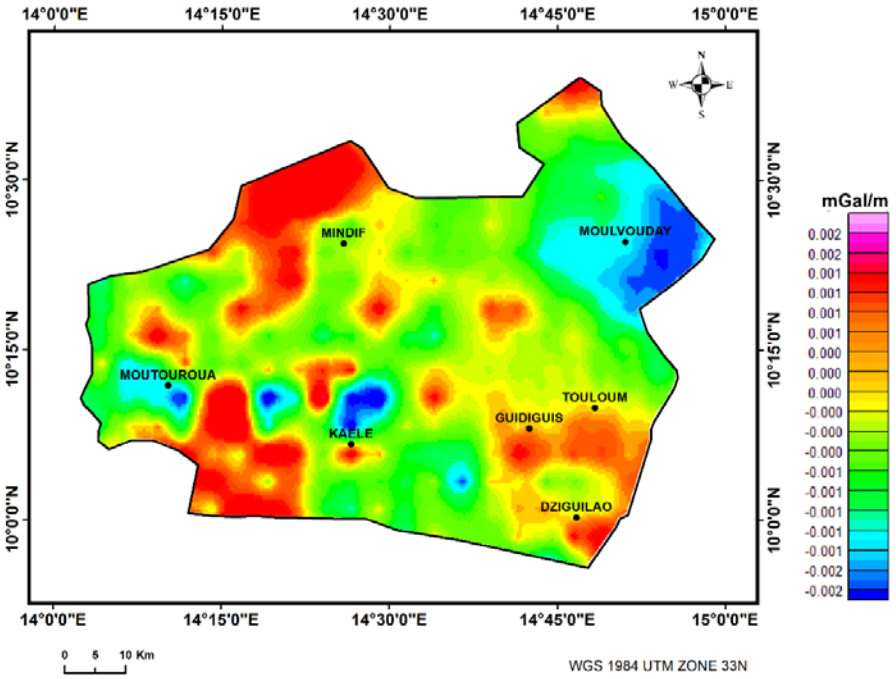

Figure 9. Vertical derivative map with maxima gradients marked in red color and minima in green, yellow and blue color

5.3. Interpretation of the Euler Solutions Map and the Fracture Map

The analysis of the lineaments represents an important step in the geological cartography of the sedimento-magmatic domains and in the prospection of the subsurface resources. Mapping by conventional methods (monitoring of faults in the field, aerial photographs according to the analogue mode) does not always allow to identify all the existing lineaments [44,45,46,47]. In this part we present the maps of Euler solutions and lineaments extracted from gravity data. These maps are fundamental in the areas of subsurface structural interpretation and mineral exploration.

5.3.1. Interpretation of the Euler's Solutions Map

Map (Figure 10) shows the set of Euler solutions obtained from the EGM2008 data. It shows the distribution of the geological structures responsible for anomalies in the region and their depths. The shallower geological structures are represented by the blue Euler solutions while the deepest structures are represented by the green and red solutions, i.e. between 1000 and 2000 m depth.

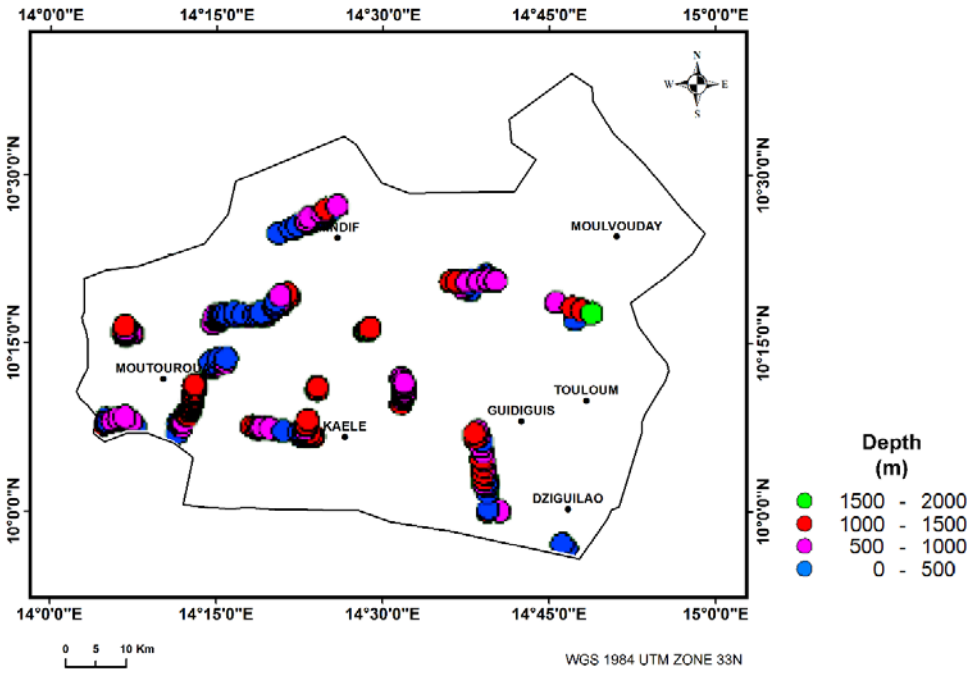

Figure 10. Euler solutions map, point distribution is an indication of the anomaly sources depth

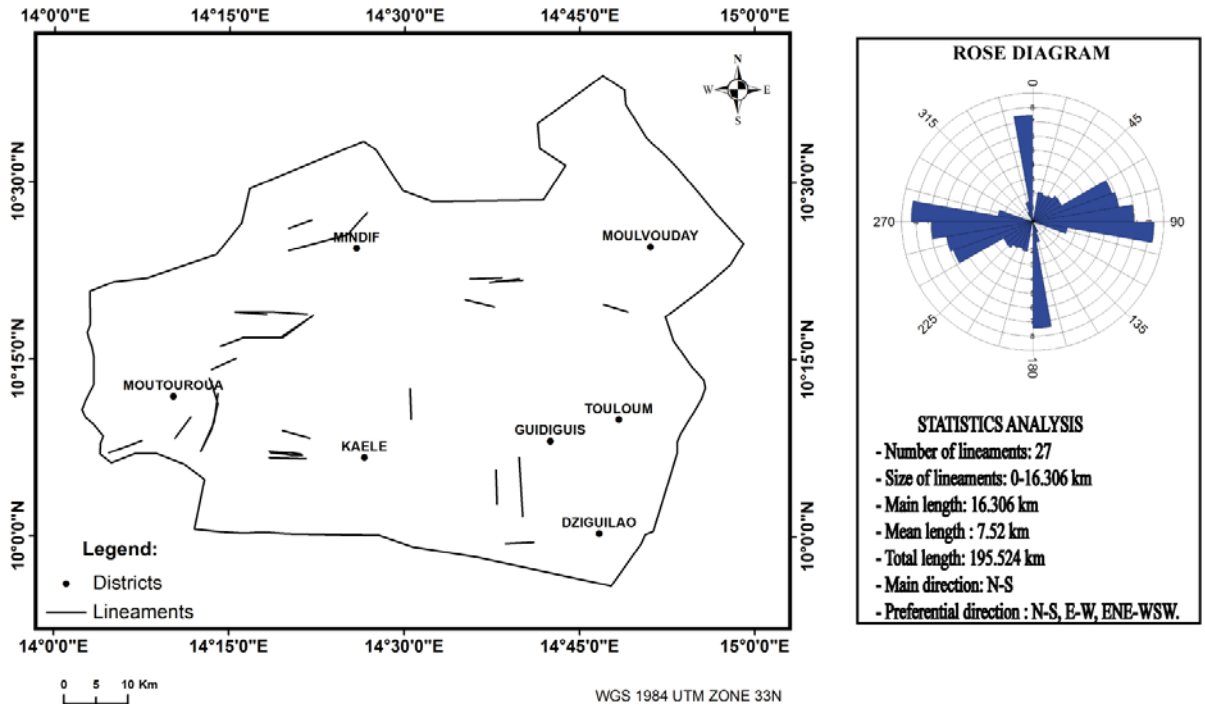

Figure 11. Fractures map. It shows the deep fracture network obtained by the gravity data

5.3.2. Interpretation of the Fracture Map

The fracture map (Figure 11) can provide information on flow directions, drainage axes and feeding areas for hydrogeological or mining research. In order to better schematize the results obtained from the polynomial separation and the horizontal and vertical derivatives, we summarize all these observations by an interpretative map of the gravity lineaments. Map (Figure 11) shows a network of lineaments that are mostly on the edge of the magmatic rock massifs. These different lineaments delimit the large geological structures of the region and confirm the field observations. The length and the density of the fracturing network represent important parameters recognized for their hydrogeological and mining interest.

The statistical analysis of the rose diagram has 27 gravity structural elements, whose size varies between 0 km at 16.306 km, the main lineaments have a length of 16.306 km, and the mean lineaments have an average length of 7.52 km. The total length of the mapped lineaments is approximately 195.524 km. The rose diagram direction highlights a main direction N-S and preferential directions: N-S, E-W ENE-WSW. This interpretation allowsto validate the interpretations already made on the residual and derivatives maps of the study area.

6. Discussion

At the scale of the Mayo-Kani region, the study of gravity maps has led to a better understanding of structural geology. This study allows to know the different deformations undergone at different scales by the rocks as well as the forces, or constraints which are the cause. The main family of structures we encountered is the faults. The Euler deconvolution solutions (Figure 10) are located at depths between 0 and 2000 m. From a qualitative point of view, the greatest depths are recorded in the infilled plain with alluvium. From a quantitative point of view, there are more shallow solutions in the areas. To validate Euler's solutions, the lineaments obtained from the deconvolution were superimposed on the geological map of the study area (Figure 2). The compilation of these lineaments and those determined by the analysis of satellite images by [27], leads to a slight parallelism. The structural interpretation of the gravity maps shows that Mayo-kani anomaly sources are located at the intersection of deep faults at depths of the order of 500 to 2000 m. These results are consistent with those obtained [27] using the Schuttler Radar Topography Mission (SRTM) data.

7. Conclusion

The purpose of this study was to map and detect structural subsurface anomalies in the Mayo-Kani Division. The application of residual regional separation to Bouguer anomaly data allowed the residual anomaly to be obtained using the third order polynomial fit. The edges and source bodies of the residual anomaly have been refined to reduce the complexity of anomalies as well as to amplify fault patterns using horizontal and vertical derivatives. The interpretation of the derived maps revealed the N-S, E-W, NE-SW and NW-SE structural trending directions. The application of the Euler Deconvolution for the detection of faults, allowed to improve the knowledge on the distribution of the geological structures source of gravity anomalies. The results obtained in this study show that the area is geologically important because it can be viable for mineral exploration and why not for hydrocarbon exploration.

Conflict of Interest

The authors declare that they have no competing interests.

Acknowledgements

This work was supported by the Department of Mines, Petroleum, Gas and Water Resources Exploration of the Faculty of Mines and Petroleum Industries of the University of Maroua, Cameroon. We thank the two referees who allowed a good consolidation of this paper.

References

[1] Fraser, A., Huggins, P., Rees, J and Cleverly, P., 1997. A satellite remote sensing technique for geological structure horizon mapping; Int. J. Rem. Sens. 18 1607-1615.

[2] Zeinalov, G.A., 2000. Importance of remote-sensing data in structural geologic analysis of oil- and gas-bearing regions of Azerbaijan; Natural Resour. Res. 9 307-313.

[3] Yassaghi, A., 2006. Integration of Landsat imagery interpretation and geomagnetic data on verification of deep-seated transverse fault lineaments in SE Zagros, Iran; Int. J. Remote Sens. 27. 4529-4544.

[4] Pavlis, N.K., Chan, J.C., and Lerch, F., 1996. Alternative estimation techniques for global high-degree gravity modeling, in Global Gravity Field and Its Temporal Variations, edited by R.H. Rapp, A.A. Cazenave, and R.S. Nerem, International Association of Geodesy Symposia, No. 116, Springer-Verlag, Berlin Heidelberg.

[5] Kiamehr, R. and Gomez-Ortiz D., 2009. A new 3D Moho depth model for Iran based on the terrestrial gravity data and EGM2008 model. GeophY'. 11, EGU2009-321-l.

[6] Arabelos, D.N and Tscheming, C.C., 2010. A comparison of recent Earth gravitational models with emphasis on their contribution in refining the gravity and geoid at continental or regional scale. J Geod, 84 (11)' 643-660.

[7] Steffen, R., Steffen, H and Jentz, K.H.G., 2011. A three-dimensional Moho depth model for the Tien Shan from EGM2008 gravity data. Tectonics, 30, TC5019,

[8] Pavlis, N.K, Holmes S A, Kenyon S C, et al., 2012. The development and evaluation of the Earth gravitational model2008 (EGM2008). Journal of Geophysical Research, 117.

[9] Bonvalot, S., Balmino, G., Briais, A., M. Kuhn, Peyrefitte, A., Vales N., Biancale, R., Gabalda, G., Reinquin, F., Sarrailh, M., 2012. World Gravity Map. Commission for the Geological Map of the World. Eds. BGI-CGMW-CNES-IRD, Paris.

[10] Yi Weiyong and Reiner Rummel., 2013. A comparison of GOCE gravitational models with EGM2008. Journal of Geodynamics, (73)' 14-22.

[11] Ngatchou Heutchi Evariste, Liu Genyou, Tahod Charles Tahod, Kamguia Joseph, Nguiya Severin, Tiedeu Alain and KE Xiaoping., 2014. Crustal structure beneath Cameroon from EGM2008, Geodesy and Geodyoamics 5(1): 1-10.

[12] Dumort, J.C and Péronne, Y., 1966. Explanatory note on the sheet of Maroua. 67p.

[13] Louis, P., 1970. Geophysical contribution to the geological knowledge of the Lake Chad Basin. bulletin ORSTOM, 42.

[14] Ewodo-Mboudou, G., Bon, A.F., Bineli E., Ntep, F., Ombolo, A., 2017. Characterization of the productivity of basement aquifers in the Far-North region, Cameroon. Journal of the Cameroon academy of sciences vol. 14 no. 1.

[15] Ngounou-Ngatcha, B., 1993. Hydrogeology of complex aquifers in semi-arid zone. Quaternary aquifers of Grand Yaere (northern Cameroon). PhD, Univ. from Grenoble I, 357p.

[16] Ngounou-Ngatcha, B., Mudry J., Wakponou, A., Ekodeck, G.E., and Sarrot Reynauld, J., 2001. The Limani-Yagoua sandy belt (North Cameroon) and its hydraulic role. J. Afr. Earth Sci., 32, 307-316.

[17] Ngako, V., Affaton, P., Nnange, J.M., Njanko, T., 2003. Pan-African tectonic evolution in central and southern Cameroon: transpression and transtension during sinistral shear movements. Journal of African Earth Sciences 36, 207-214.

[18] Penaye, J., Toteu, S.F., Tchameni, R., Van Schmus, W.R., Tchakounté, J., Ganwa, A., Minyem, D., Nsifa, E.N., 2004. The 2.1 Ga West Central African belt in Cameroon. Journal of African Earth Sciences 39, 159-164.

[19] Tchameni, R., Pouclet, A., Penaye, J., Ganwa, A. A., Toteu, S.F. 2006. Petrography and geochemistry of the Ngaoundéré Pan-African granitoids in Central North Cameroon: Implications for their sources and geological setting. Journal of African Earth Sciences 44/4-5, 511-529.

[20] Penaye, J., Kröner, A., Toteu, S.F., Van Schmus, W.R., Doumnang, J.C., 2006. Evolution of the Mayo-Kebbi region as revealed by zircon dating: an early (ca. 740 Ma) PanAfrican magmatic arc in southwestern Chad. Journal of African Earth Sciences 44, 530-542.

[21] Ngako, V., Affaton, P., Njonfang, E., 2008. Pan-African tectonics in northwestern Cameroon: implication for the history of western Gondwana. Gondwana Research 14, 509-522.

[22] Njanko, T., Nédélec, A., Kwékam, M., Siqueira, R., Esteban, L., 2010. Emplacement and deformation of the Fomopéa pluton: implication for the Pan-African history of Western Cameroon. Journal of Structural Geology 32, 306-320.

[23] Ganwa, A.A, Siebel, W., Frisch, W., Shang, C.K., 2011. Geochemistry of magmatic rocks and time constraints on deformational phases and shear zone slip in the Méiganga area, central Cameroon. International Geology Review 53, 759-784.

[24] Moussa, I., 2011. Neoproterozoic crustal growth and differentiation: example of the Mayo-Kebbi pan-African domain in southwestern Chad. University Henri Poincaré, Nancy, France, pp. 339, Ph.D. Thesis.

[25] Kouske, A.P., Suh, C.E, Ghogomu, R.T., Ngako, V., 2012. Na-Metasomatism and Uranium Mineralization during a Two-Stage Albitization at Kitongo, Northern Cameroon: Structural and geochemical evidence. International Journal of Geosciences 3, 258-279.

[26] Moussa, I., André-Mayer, A.S., Vanderhaeghe, O., Barbey, P., Deloule, E., 2012. A-type granites from the Pan-African orogenic belt in south-western Chad constrained using geochemistry, Sr–Nd isotopes and U–Pb geochronology. Lithos 153, 39-52.

[27] Wambara, B., Wapouo, R. and Djimeli, A., 2017. Contribution of remote sensing and geographic information system to geological mapping and minerals exploration in the region of Mayo-Kani (Cameroon). Academic Internship Report 60p.

[28] Bosch, W., 1993. A rigorous least squares combination of low and high degree spherical harmonics, presented at the IAG General Meeting, Beijing, People's Republic of China.

[29] Malys, S., 1996. The WGS84 Reference Frame, National Imagery and Mapping Agency, November 7.

[30] Smith, D.A., and D.G. Milbert, 1997a. Evaluation of preliminary models of the geopotential in the United States, in Bulletin of the International Geoid Service.

[31] Smith, D.A., and D.G. Milbert, 1997b. Evaluation of the EGM96 model of the geopotential in the United States, in Bulletin of the International Geoid Service.

[32] Sideris, M., 1997. International tests of the new GSFC/DMA geopotential models, in Gravity, Geoid and Marine Geodesy, International Symposium, Tokyo, September 30–October 5, 1996, Segawa, Fujimoto, and Okubo (ed.), International Association of Geodesy Symposia, Vol. 117, Springer–Verlag.

[33] Geosoft Oasis Montaj., 2008. The core software platform for working with large volume gravity and magnetic spatial data; Geosoft Inc, Toronto, Canada.

[34] Gupta, V.K., 1983. A Least Squares Approach to Depth Determination from Gravity Data. Geophysics 48: 357-360.

[35] Murthy, I.V.R and Krisshnamacharyulu, S.K.G., 1990. A Fortran 77 Programme to Fit a Polynomial of Any Order to Potential Field Anomalies. Journal of Association of Exploration Geophysicists 11: 99-105.

[36] Nguimbous-Kouoh, J.J., Ngos III, S., Mbarga, T.N, Manguelle-Dicoum E., 2017. Use of the Polynomial Separation and the Gravity Spectral Analysis to Estimate the Depth of the Northern LogoneBirni Sedimentary Basin (Cameroon). International Journal of Geosciences 8: 14-42.

[37] Grauch, V.J.S., Bauer, P.W. and Kelson, K.I., 2004. Preliminary Interpretation of High-Resolution Aeromagnetic Data Collected near Taos, New Mexico. New Mexico Geological Society, 55 th Field Conference, Guidebook, 244-256.

[38] Verduzco, B., Fairhead, J.D., Green, C.M. and Mac Kenzie, C., 2004. New Insights into Magnetic Derivatives for Structural Mapping. The Leading Edge, 23, 116-119.

[39] Cooper, G.R.J and Cowan, D.R., 2006. Enhancing potential field data using filters based on the local phase; Comput. Geosci. 32 1585-1591.

[40] Salem, A., William, S., Fairhead, D., Ravat, D. and Smith, R., 2007. Tilt-Depth Method: A Simple Depth Estimation Method Using First-Order Magnetic Derivatives. The Leading Edge, 150, 2-5.

[41] Salem, A., Williams, S., Faihead, J.D., Smith, R and Ravat, D., 2008. Interpretation of magnetic data using tilt-angle derivatives; Geophysics 73 L1-L10.

[42] Reid, A.B., Allsop, J.M., Granser, H., Millett, A.J. and Somerton, I.W., 1990. Magnetic Interpretation in Three Dimensions Using Euler Deconvolution. Geophysics, 55, 80-90.

[43] Durrheim, R.J. and Cooper, R.J., 1998. A Program for the Euler Deconvolution of Magnetic and Gravity Data. Computer and Geosciences, 24, 545-550.

[44] Mnissar H.S., 2002. Contribution of remote sensing and geographic information system to geological mapping and oil exploration in the region of the Eastern High Atlas (Morocco). PhD Thesis, Mohammed V University, Fac. Sci. Rabat.

[45] Chen, S and Zhou, Y., 2005. Classifying depth-layered geological structures on Landsat TM images by gravity data: A case study of the western slope of Songliao Basin, northeast China; Int. J. Remote Sens. 26 2741-2754.

[46] Vanié, L.T.A., Khattach, D., Houari, M.R., Chourak, M. and Corchete, V., 2006. Contribution of the gravity filtering anomalies in the determination of the major tectonic accidents of the Anti-Atlas (Morocco), Proceedings of the 3rd Maghrebian Symposium of Applied Geophysics. Oujda May 11-13, 2006, 23-30.

[47] Cengiz, O., Sener, E and Yagmurlu, F., 2006. A satellite image approach to the study of lineaments circular structures and regional geology in the Golcuk Crater district and its environs (Isparta, SW Turkey); J. Asian Earth Sci. 27(2) 155-163.

[48] Bouiflane, M., 2008. Aeromagnetic and magnetic multi-scale mapping: structural study of a region of the Rhenan moat. PhD Thesis, Louis Pasteur University, Strasbourg 1.

[49] El Gout, R., Khattach, D. and Houari, MR., 2009. Gravity study of the northern flank of Béni Snassen (Eastern North Morocco): structural and hydrogeological implications. Mohamed Premier University, Oujda. Bull. Ins Sci., Rabat, Earth Sciences Section, 31, 61-75.

[50] Basseka, C.A., Shandimi, Y. and Tadjou, J.M., 2011. Subsurface Structural Mapping Using Gravity Data of the Northern Edge of the Congo Craton South Cameroon. Geofizika, 29, 229-245.

[51] Reid, A.B. and Thurston, J.B., 2014. The Structural Index in Gravity and Magnetic Interpretation: Errors, Uses, and Abuses. Geophysics, 79, J61-J66.